VENTILATION PERFORMANCE AND POLLUTANT FLOW IN A UNIDIRECTIONAL-TRAFFIC ROAD TUNNEL

by

Milan B. ŠEKULARAC[a] , Novica Z. JANKOVIĆ[b*], and Petar V. VUKOSLAVČEVIĆ[a]

[a]Laboratory for Energy Processes, Faculty of Mechanical Engineering,
University of Montenegro, Podgorica, Montenegro
[b]Hydraulic Machinery and Energy Systems Department, Faculty of Mechanical Engineering,
University of Belgrade, Belgrade, Serbia

Original scientific paper
https://doi.org/10.2298/TSCI160321117S

To develop a reliable method for modeling fire case scenarios within the road tunnels and observing the effects of the skewed velocity, experimental and numerical approach is used. Experimental results obtained from a laboratory tunnel model installation, are used to define geometry and boundary conditions. The result for the overall ventilation performance is compared to the available cases, for empty tunnel and stationary bi-directional vehicle traffic. For a unidirectional traffic road tunnel, in traffic loaded conditions, with a ventilation system based on axial ducted fans, the numerical simulation is used to determine the flow and temperature fields, the ventilation efficiency (efficiency of momentum transfer), and to assess the shape of the velocity distribution. The effect that a skewed velocity distribution can have on the resulting thermal and pollutant fields (CO_2), smoke backlayering and stratification, is evaluated using numerical simulations, for the model-scale tunnel fire conditions. The effect of two possible limiting shapes of the velocity distribution, dependent only on the location of the fire with respect to the nearest upstream operating fans, is analyzed. The numerical results for a fire are scenario are a starting point in assessing the feasibility of a laboratory model fire-scenario experiment, what is planned as the next step in this research.

Key words: traffic tunnel, ventilation efficiency, axial ducted fans, boundary conditions, fire

Introduction

The tunnel with unidirectional-traffic occurring in two road lanes is analyzed. The ventilation system considered here is designed by utilizing axial ducted fans mounted on the tunnel ceiling, which is the most common layout in the possible configurations. A review of possible design concepts for traffic tunnel ventilation installation and fan design advances can be found [1, 2].

The case of congested traffic is taken to occur at typical low vehicle speed of ~10 km/h, considered here. Such scenario is of particular interest, since the largest air demand occurs at low vehicle speeds and the number of the vehicles in the tunnel is normally the largest, whereas the vehicle pollutant emission is also the highest [3]. The vehicle num-

* Corresponding author, e-mail: milans@ac.me

ber increases the overall hydraulic resistance in the tunnel, thus making the congested traffic case relevant for sizing of the installation [3].

In order to evaluate the efficiency of momentum transfer in the specific case considered, the following definitions are used: the fan static thrust T, the tunnel-exerted effective thrust, T_{ef}, and the tunnel air-stream thrust using Darcy law formulation augmented with local resistances of moving vehicles T_{efd} [2, 3]:

$$T = \rho A_f w^2 \tag{1}$$

$$T_{ef} = NT\left(1 - \frac{v_t}{w}\right)\eta_i = NTk_1\eta_i \tag{2}$$

$$T_{efd} = \left(\zeta_{in} + \xi\frac{L_t}{D_h} + 1\right)A_t\rho v_t^2/2 + \sum_{i,veh}\zeta_i A_i\rho(v_i - v_{v,i})^2/2 \tag{3}$$

where w, v_t, A_f , v_v, and ζ_i are the mean axial velocity of the fan's jet, the air mean-velocity, the fan's exit cross-section area, the absolute value of vehicle velocity, and the hydraulic resistance coefficient of the vehicle, respectively. The factor k_1 denotes the influence of the mean axial velocity of the tunnel flow which offloads the fan, and η_i factor is usually referred to as the efficiency of momentum transfer from fan jets to the air stream or installation efficiency [1, 3, 4]. Factor k_1 can be increased only by increasing the velocity of the jet at the fan exit. The overall energy efficiency of the ventilation system is influenced by the hydraulic efficiency of the fan (0.40-0.80), the motor efficiency (≈ 0.90 - 0.95), and the efficiency of momentum transfer η_i. The η_i and velocity profile is determined for empty tunnel air flow using laboratory tunnel-model experiments and CFD which was successfully validated [3]. For this purpose, experimentally determined turbulent flow at the exit of the used axial ducted fans, obtained using hot-wire anemometry, was used as a boundary condition [3, 5] in numerical simulations.

From an empty tunnel flow analysis, it was determined in [3] that the properties of the generated fan flow (the CFD boundary conditions) influence the velocity distribution and the η_i efficiency by up to 9%. Possible fan-jet tilting or use of tilted nozzles can affect the axial velocity distribution additionally [6].

Tunnel model and boundary conditions for flow simulation

The experimental installation is presented in fig. 1. It consists of a main and escape tunnel. It is designed for the analysis of bidirectional-traffic as it is described in [3, 5]. It can also serve for the analysis of ventilation of unidirectional traffic tunnel as it is done in this work. In order to perform fire scenario experiments the model is equipped with Keithley 40-thermocouple system, 5 CO_2 Meter CO_2-transducers, and a LPG burner. The characteristic distance L between fan batteries (in the downstream direction is approx. 5 m ≈ 100 $D_f \approx D_h$. At $L_m = 4L = 20.52$ m the installation corresponds to approx. $L_{ob} = 400$ m of a real-scale tunnel. The utilized fans are UAV propulsion axial fans by Great Planes, model Hyperflow with a 55 mm rotor diameter. The interpolated time-averaged velocity components (axial, radial, and tangential) of the fan generated flow field at fan's exit are given in figs. 2 [3, 5]. Mean values (flow-weighted) of time-averaged dimensionless velocity components $v_i^* = v_i/w$ with $w = 34.5$ m/s are: v_z, v_r, v_t = 1, 0.041, 0.053, and the corresponding values of yaw α and pitch β angles are: 3° and 2.3°, respectively.

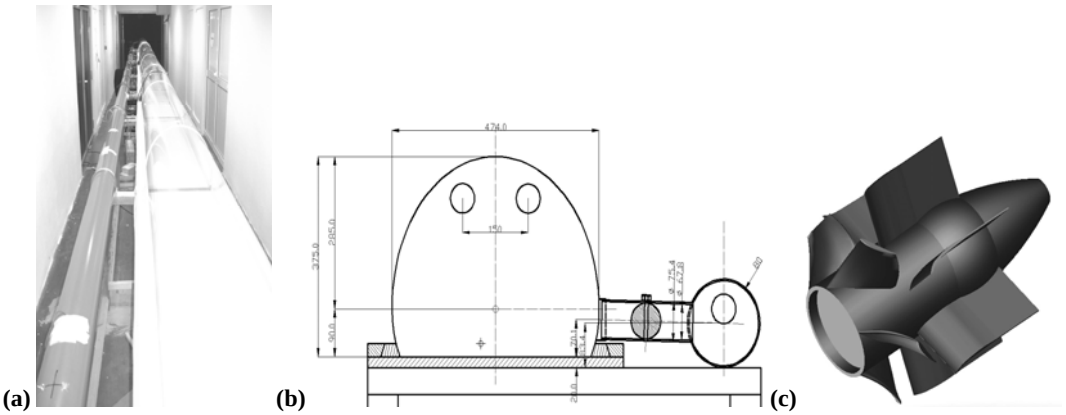

Figure 1. Installation; (a) Installation photo, (b) cross-section, and (c) the fan

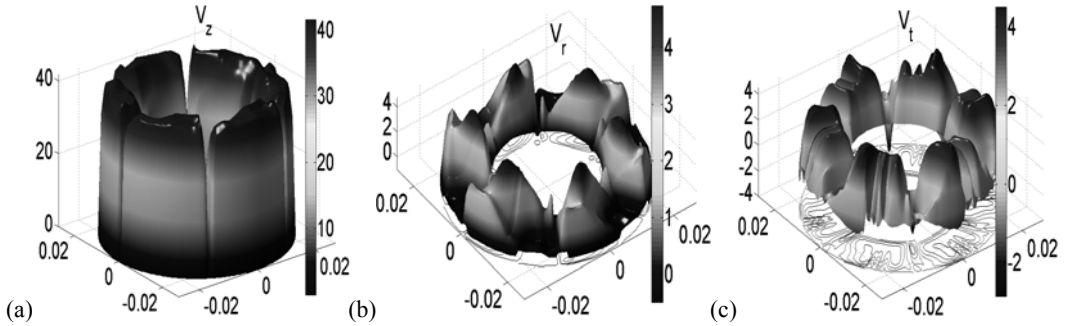

Figure 2. Time-averaged velocity components of fan exit turbulent field; (a) axial v_z, (b) radial v_r, and (c) tangential v_t

The TKE field used to set up the boundary conditions on fans (and other experimental results of used fans) can be found in [3, 5]. Recent numerical approaches in computing flow and temperature field in transient conditions in tunnels are based on multi scale modeling [7].

Numerical results

The CAD model and the numerical grid

The generated CAD model with fans corresponds to the laboratory scale tunnel model, fig. 3. A hybrid CV grid with $\approx 9 \cdot 10^6$ elements in the fluid-domain, consisting of prismatic and tetrahedral finite volumes was generated, with surfaces around solids (fan, tunnel wall, vehicles-models) covered by 10-15 layers of inflated prismatic cells, and the rest of the domain covered with tetrahedral cells. The cell size spans from ≈1 mm (which is ~50% of the mean value of integral length scales of the fan turbulent flow) up to ~25 mm (~ 6% of tunnel hydraulic diameter) far from the fans, which can provide proper accuracy. The wall-normal size of prismatic cells at the walls was fine enough to provide an average $y^+ \sim 1$.

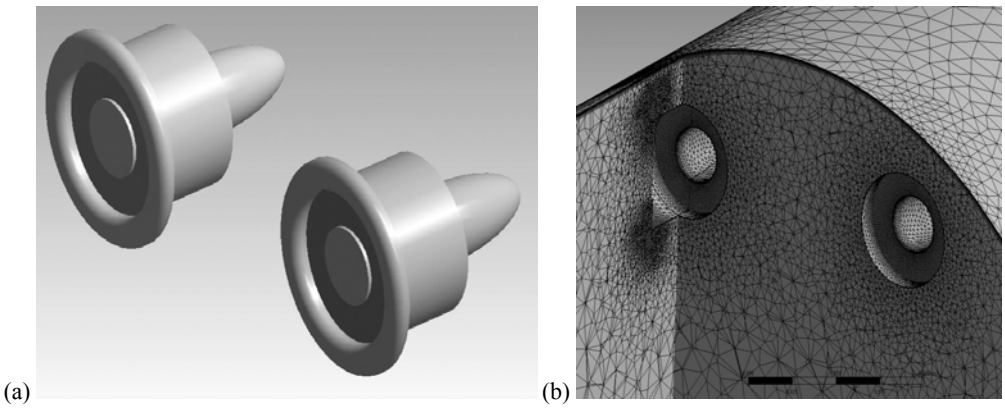

Figure 3. The CAD and grid; (a) CAD model and (b) grid cutout

Mathematical model and numerical approach

Flow was computed by numerically solving a system of incompressible Reynolds-averaged Navier-Stokes (RANS) equations in the Fluent code, which is based on the finite-volume discretization method [3, 8]:

$$\frac{\partial \overline{v}_i}{\partial x_j} + \frac{\partial(\rho \overline{v}_i \overline{v}_j)}{\partial x_j} = -\frac{\partial \overline{p}}{\partial x_j} + \mu \frac{\partial^2 \overline{v}_j}{\partial x_j^2} + \frac{\partial R_{ij}}{\partial x_j} + f_i \tag{4}$$

$$\frac{\partial \rho}{\partial t} + \frac{\partial(\rho \overline{v}_i)}{\partial x_i} = 0 \tag{5}$$

where $R_{ij} = -\overline{\rho v_i' v_j'}$ is the Reynolds turbulence stress tensor which has to be modeled. Turbulence was modeled using standard k–ε turbulence model, and the enhanced wall function approach. All the model constants had their default values: $C_\mu = 0.09$, $C_{1\varepsilon} = 1.44$, $C_{2\varepsilon} = 1.92$, $P_{rk} = 1$. The iterative procedure was carried until all the residuals were reduced to10-5, and integral quantities showed no further change. The adopted vehicle share is approx. 30% of large vehicles (model buses) *vs*. model passenger cars. Thus the number of vehicles in the analyzed CFD tunnel model was: 38 passenger cars and 12 buses. The vehicles are assumed to move at ≈ 2.78 m/s, thus a moving wall condition was prescribed for vehicle surfaces. The obtained results represent an averaged (quasi-steady) result of the flow field. Fluid physical properties for isothermal case were $\mu = 1.8 \cdot 10^{-5}$ Pa·s, $\nu = 1.5 \cdot 10^{-5}$ m^2/s $\rho = 1.2378$ kg/m^3, and correspond to conditions of laboratory experiments in [3]:

$$\frac{\partial}{\partial t}(\rho \overline{f}) + \nabla \cdot (\rho \vec{v} \overline{f}) = \nabla \cdot (\frac{\mu_t}{\sigma_t} \nabla \overline{f}) + S_m + S_{user} \tag{6}$$

$$\frac{\partial}{\partial t}(\rho \overline{f'^2}) + \nabla(\rho \vec{v} \overline{f'^2}) = \nabla \cdot \left(\frac{\mu_t}{\sigma_t} \nabla \overline{f'^2} \right) + C_g \mu_t + \left(\nabla \overline{f} \right)^2 - C_d \rho \frac{\varepsilon}{k} \overline{f'^2} + S_{user} \tag{7}$$

Implicit second-order time-marching was used to integrate the equations in time, using a time step: $\Delta t = 0.03$ s to keep the overall CFL < 1. The normalized residuals of the equation were reduced to about $5 \cdot 10^{-5}$-$5 \cdot 10^{-6}$.

The CFD results for isothermal air flow with unidirectional traffic

Two cases are studied: S1 with the fans operating and S2 with a known inlet velocity v_t prescribed. Typical parameters of the cases S1 and S2 are given in tab. 1; both are computed as steady.

Vehicles generate a hydraulic resistance which is not known accurately a priori. In the S2 case, the thrust can be also exerted by an outside source, or it can be assumed as thrust exerted by sufficiently far away fans positioned much further upstream. Thus the inlet air velocity was considered at (constant) profile, and the value was taken equal to the obtained mean value of axial velocity in S1 case (with fans working). This way it was possible to estimate the effective pressure drop (or thrust) exerted on the air in such hydraulic conditions in the tunnel, required to generate the equal mean air velocity. Comparing this thrust to the inputted ventilation thrust in S1 case, multiplied by a reduction factor k_1, using eq. 2, the efficiency of the ventilation in S1 scenario was estimated. Velocity distribution in S1 case with operating fans is given in fig. 4. To compare axial-velocity distribution, along the height above the road-surface y/y_{max}, in cases S1 and S2, the values were extracted at 13 different equidistant cross-sections D_h apart, along the furthest-downstream portion of the CFD tunnel, fig. 5. The computed effective value of $\eta_i \approx 0.71$, is lower than for the empty tunnel air flow case (≈0.80).

Table 1. Cold flow CFD data

Case	v_t	k_1	η_i	Boundary conditions
S1	4.897	0.858	0.71	v_x,v_y v_z, *TKE*
S2	4.897	–	–	inlet $v_t \equiv v_t$ (S1)

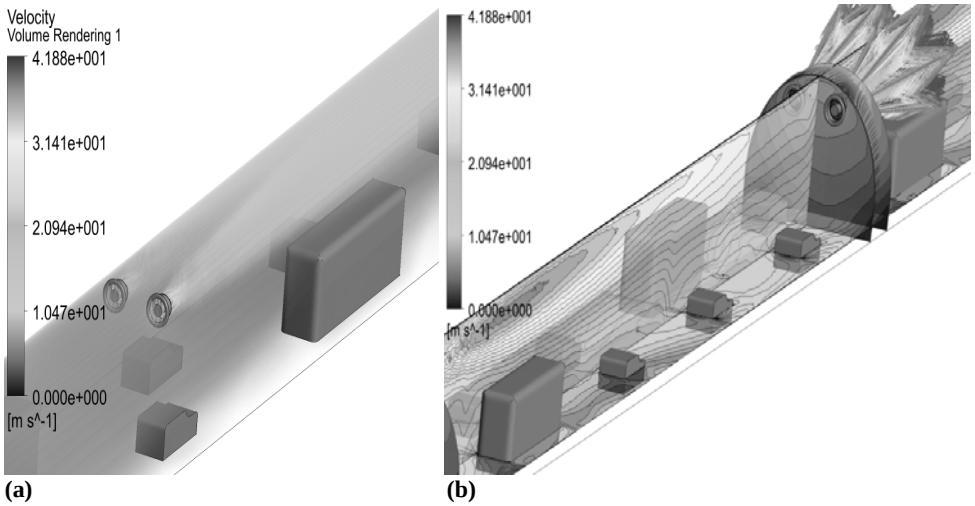

(a) **(b)**

Figure 4. Velocity field in S1-case; (a) volume rendering and (b) vectors in a fan-outlet cross-section *(for color image see journal website)*

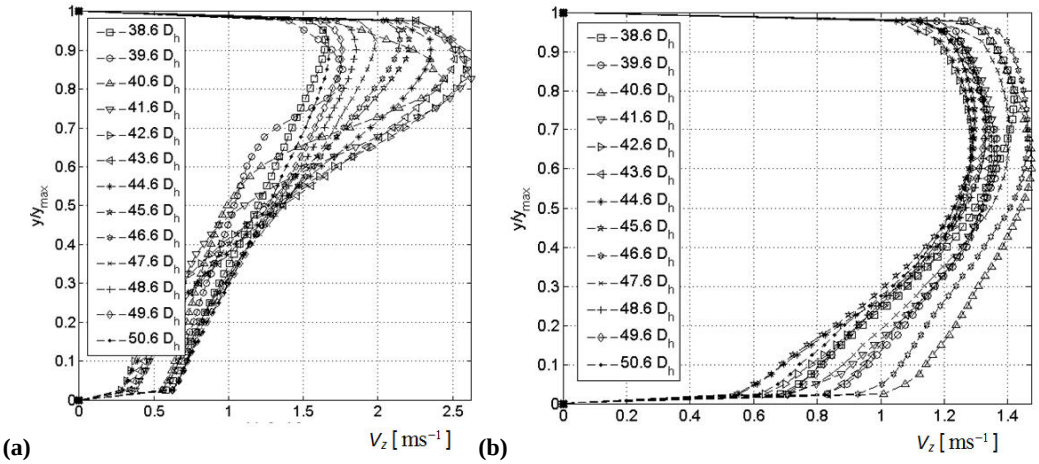

Figure 5. Profile of dimensionless axial velocity ($v_z = v_t$) *vs.* height ($y = H$); (a) S1-case, (b) S2-case: profiles are extracted along the last tunnel-segment (100 D_f long)

Effects of flow in a tunnel fire scenario

Model geometry and boundary conditions

To evaluate the effect that the velocity distribution can have on the smoke flow and temperature fields, a fire-tunnel segment of 20 tunnel hydraulic diameters D_h long without fans, downstream of the previously considered segment was used. The fire was produced by injecting gas fuel from a burner (12 mm opening tube), fig. 6, in the midpoint of the fire-tunnel segment (at $z = 10\ D_h$) at road surface level (180 D_f downstream of the last operating fan battery). Two pairs of CFD-cases were computed: (S3.1-S3.2) and (S4.1-S4.2). In (S3.1-S3.2) the heat release rate corresponds to a single passenger car-fire: 1.34 kW, or for tunnel-object scale ($H_{ob} \approx 7$ m) conditions $(\dot{Q}_m / \dot{Q}_{ob} = (H_m / H_{ob})^{5/2})$ is $\dot{Q}_{ob} = 2$ MW.

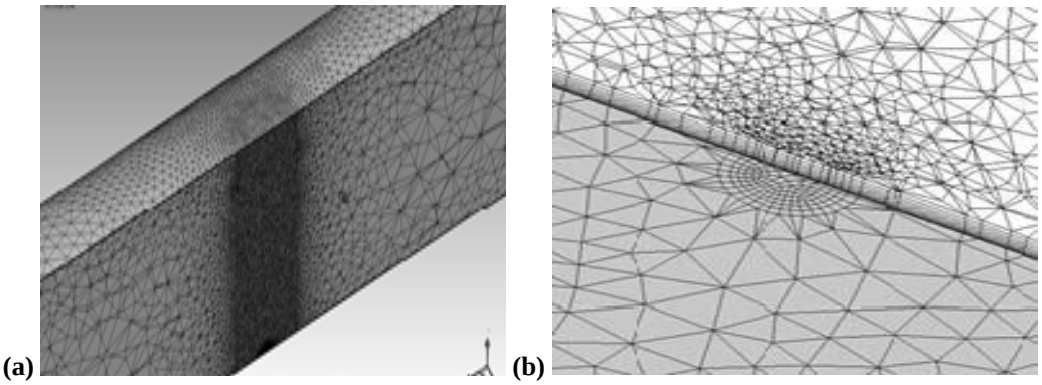

Figure 6. Numerical grid for the fire-scenario cases; (a) vertical symmetry slice, (b) detail of fuel entry hole

A good overview of the results on fire safety in road tunnels can be found in [9]. To estimate the critical velocity for smoke control, the following expressions for critical velocity and fire heat-release rate, obtained from the experimental results of [10] are used:

$$v_{cr}^{*} = \frac{v_{cr}}{\sqrt{gH_h}} = \begin{cases} 0.4\left(\dfrac{\dot{Q}^{*}}{0.2}\right)^{1/3}, & \text{if } \dot{Q}^{*} \le 0.2 \\ 0.4, & \text{if } \dot{Q}^{*} > 0.2 \end{cases} \tag{8}$$

$$\dot{Q}^{*} = \frac{\dot{Q}}{\rho_0 c_p T_0 g^{1/2} H_h^{5/2}}, \tag{9}$$

where ρ_0 and T_0 are air density and temperature at tunnel entry, c_p the air specific heat and H_h, according to [10], should be taken as the tunnel hydraulic diameter $H_h = D_h$, not the tunnel ceiling height H.

The velocity for fire-cases (S3.1-S3.2) was selected to be 50% lower than v_{cr} at corresponding $\dot{Q}$, to allow for smoke back-layering to occur in numerical solutions of (S3.1-S.3.2). In both (S3.1, S3.2) the v_t is equal, but in S3.1 the inlet velocity field is a flat (constant) profile whereas in S3.2 the velocity field is a scaled representation of the computed skewed distribution at tunnel outlet in S1 case. The (S4.1-4.2) cases are designed in equal way, but using a much larger fire size, corresponding to a scaled bus or HGV (heavy goods vehicle) heat release rate: $\dot{Q}$ = 13.285 kW (or $\dot{Q}$ = 20 MW at object-scale), and to be at the critical conditions of smoke control. The critical velocity v_{cr} was obtained from eqs. 8 and 9 [10]. The S4.1 case corresponds to the at velocity profile at tunnel entry whereas for S4.2. a scaled representation of the computed skewed velocity distribution, determined in S3.1 for tunnel outlet, was used as tunnel-entry field. The selected input-data are given in tab. 2.

Table 2. Fire-scenario CFD cases data

Case	$\dot{Q}$ [kW]	v_t [ms^{-1}]	v_{cr} [ms^{-1}]	B.C. (tunnel entry)
S3.1	1.34	0.156	0.31	flat
S3.2	1.34	0.156	0.31	skewed
S4.1	13.28	0.156	0.67	flat
S4.2	13.28	0.156	0.67	skewed

Propane (C_3H_8) gas-fuel was used for (S3.1-S3.2), and a mixture of 65% propane (C_3H_8) − 35% butane (C_4H_{10}) was used for S4.1-S4.2. Initial, entry-air and fuel temperatures of 280 K, air density of 1.225 kg/m^3 were taken for all computed cases. Tunnel wall were considered adiabatic. The grid consisting of $\approx 1.1 \cdot 10^6$ CV's was refined above the fuel-entry hole (within an imaginary cylinder-body) with cell size limited to 5 mm (~1% of D_h).

Numerical results for S3.1 and S3.2 cases. Velocity streamlines at t = 30 s, just prior to the smoke backlayering front reaching the upstream air inlet, are presented in fig. 7.

Corresponding dimensionless time is defined as: $t^{*} = t/t_{ref}$, with $t_{ref} = D_h/v_t$. Temperature stratification is presented in fig. 8. Temperature value T = 333 K ≈ 60 ºC and CO_2 concentration value r_{CO_2} = 1 %, are used as characteristic for estimating the extents of the unsafe

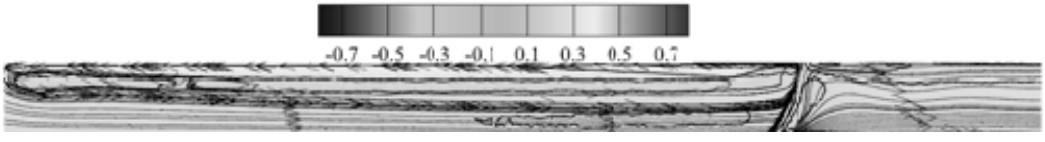

Figure 7. Velocity streamlines, and v_z contours in S3.1 after t^{*} = 12 *(for color image see journal website)*

– polluted volume. In fig. 9, the CO_2 distribution is presented by contours of concentration in the tunnel-symmetry plane, after $t^* = 12$ from the fire initiation. The difference in temperature and pollutant field for the scaled passenger-vehicle fire size ($\dot{Q}$ = 1.34 kW) cases is rather small. The back-layering front in the S.3.1 case reaches the upstream tunnel entry slightly prior to S3.2. By comparing the temperatures of S3.1 *vs*. S3.2, slight differences appear: lower temperatures downstream of the fire plume (in S3.1), but higher temperatures in the upstream back-layering smoke front (S3.2), fig. 8(b).

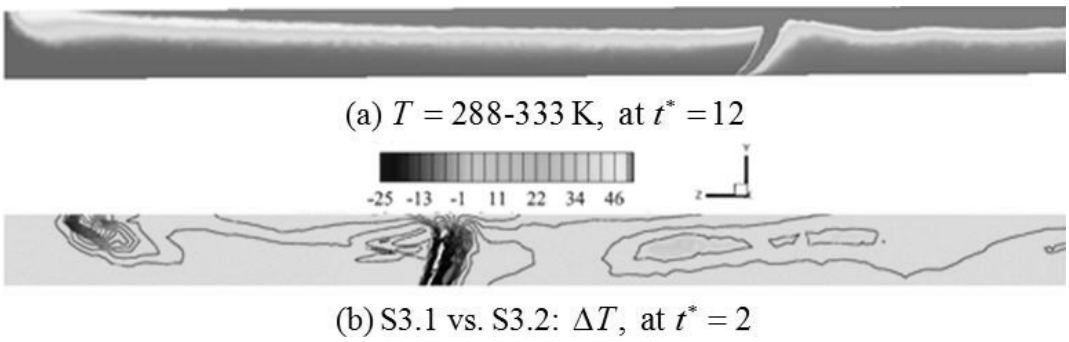

Figure 8. (a) Temperature stratification in the tunnel symmetry plane *Ozx*, at $t^* = 12$ (T = 280-333 K), (b) S1 vs S2 comparison at $t^* = 2$: temp. differences ($T_{S.3.1} - T_{S.3.2}$) *(for color image see journal website)*

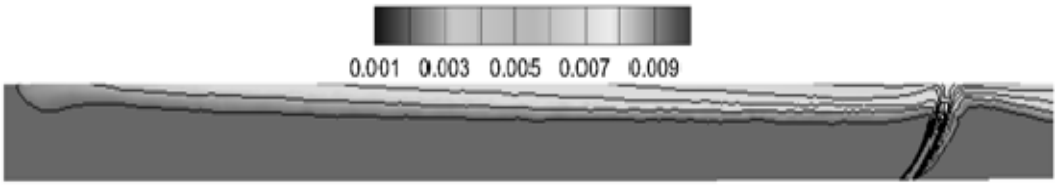

Figure 9. Contours of r_{CO_2} = 0-1% in the vertical tunnel-symmetry plane
(for color image see journal website)

Numerical results for S4.1 and S4.2 cases. The differences in pollutant and temperature fields, between these two flow conditions, are more pronounced for higher heat release rates. The velocity modulus distribution in the vertical symmetry plane, for S4.2. case, is given in fig. 10.

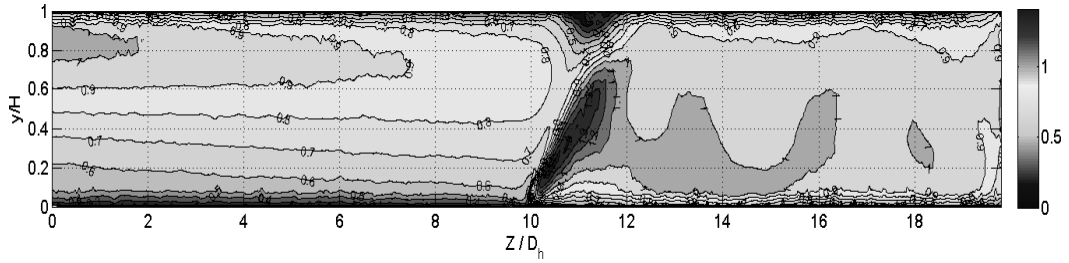

Figure 10. Velocity modulus in tunnel-symmetry plane ($t^* \approx 50$) S4.2 case
(for color image see journal website)

Vertical velocity component v_y for S4.2 case, in horizontal plane at scaled average person height (1.75 m), *i. e.* ≈ 23 % of tunnel height H, is given in fig. 11. The temperature field developed in the tunnel downstream of the fire source, for vertical symmetry plane, is given in fig. 12.

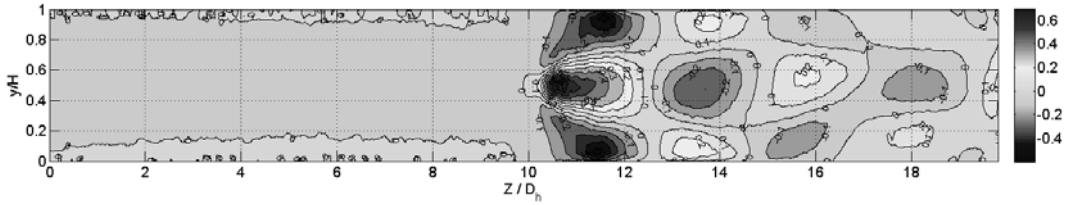

Figure 11. Vertical velocity v_y for S4.2 case in the horizontal plane (y/H = 0.23)
(for color image see journal website)

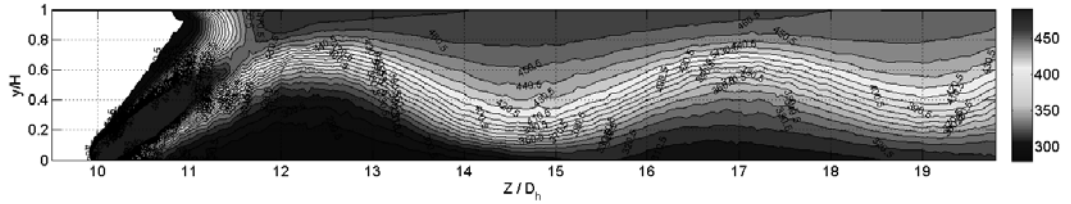

Figure 12. Temperature distribution in the vertical symmetry plane for S4.2 case
(for color image see journal website)

By proper averaging of the pollutant and temperature fields, it was possible to assess the overall distribution and the resulting differences. The stratified temperature distribution, for the vertical tunnel symmetry-plane, was averaged horizontally, per given height. The values were taken for axial positions from the burner axis downstream (*i. e.* z/D_h = 10-20). The computed average distribution of the temperature is given in fig. 13 for the two considered cases. It is clear from fig. 13(c) that approx. 15% higher value of relative temperature increase occurs in S4.2 case, at scaled average person height.

The pollutant movement for the two cases analyzed here, is compared in fig. 14, where the cloud of iso-concentration (r_{CO_2} = 1 %) is presented.

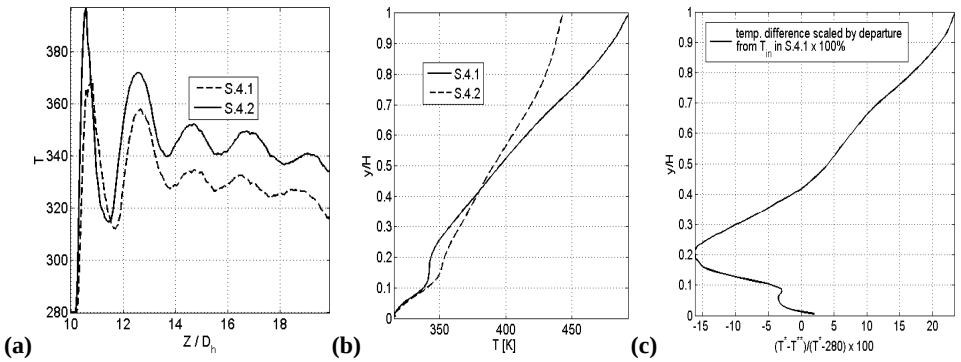

Figure 13. Comparison of axial temperature distribution downstream of the burner (located at z/D_h = 10); (a) Temperatures in the horizontal plane (y = 0.23H), averaged in the x-wise direction *vs.* axial position z/D_h, (b) Temperatures in the symmetry plane, horizontally-averaged downstream of the burner axis, vs. height $y = H$, and (c) Relative difference in temperature for the two cases (T^*, T^{**} correspond to S4.1, S4.2, respectively), scaled by the departure of the S4.1-case temperature from the air entry-temperature T_1 = 280 K, in %

The cloud is contoured with the values of temperature, taken in the range 500-550 K. The average CO_2 concentration at a horizontal plane $y/H = 0.23$ height above the road, averaged downstream of the burner, is approx. 26 % higher in the S4.2 case (skewed velocity distribution at tunnel entry) than in S4.1. For the mid-height ($y/H = 0.5$) plane, the values are of similar order, with the averaged pollutant concentration value slightly higher, by 6%, in the S4.1 (at entry velocity profile) case. The axial velocity for the at entry velocity profile case (S4.1) extracted at 4 %H under the ceiling, shown in fig. 14(c), approaches the value of 0 exactly above the fire source (burner axis at $z/D_h = 10$), and has a negative value in a backward oriented vortex downstream of the burner (for $z = D_h \approx 10 - 11.75$) before becoming positive again. The CO_2 and T values show the increase from the fire source position downstream. These results are in a very good agreement with the experimental results performed for critical conditions presented in [10].

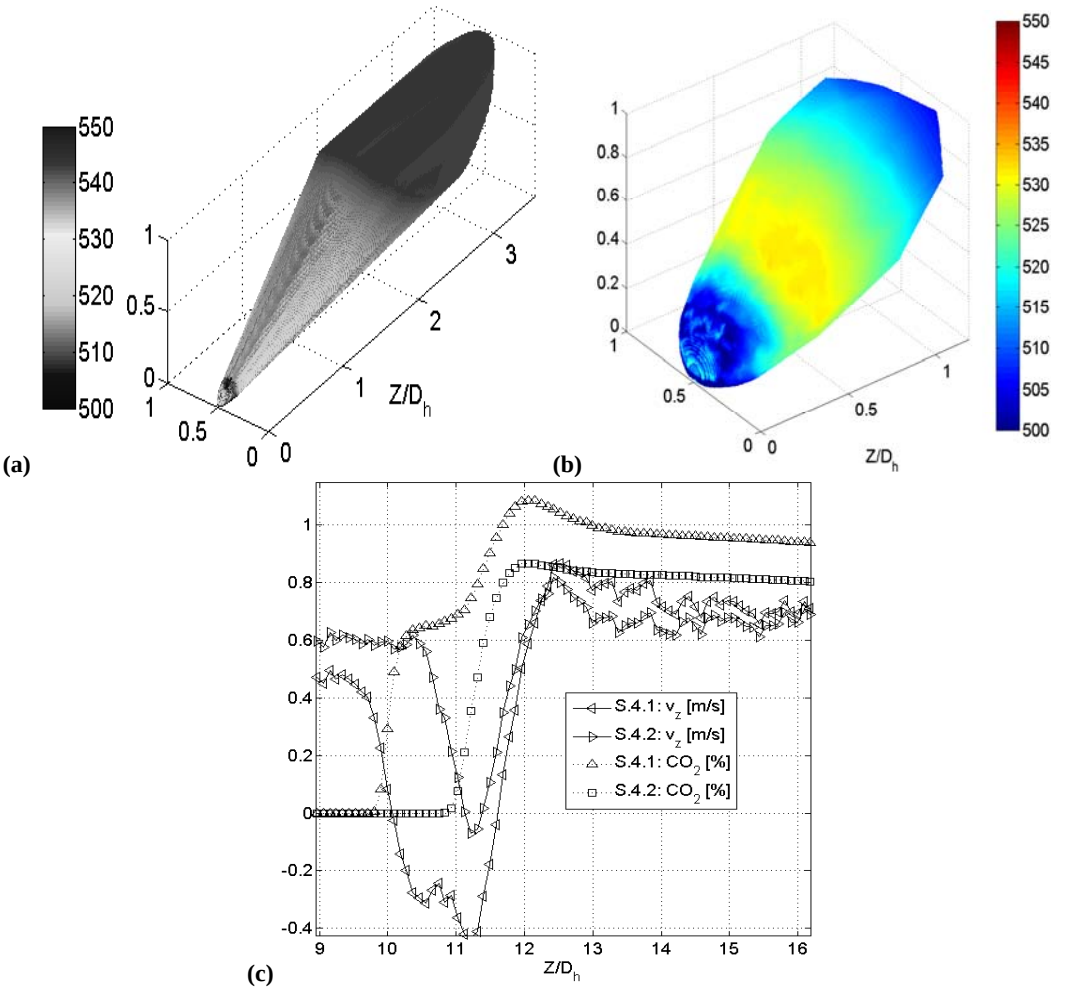

Figure 14. Pollutant distribution downstream of the fire source; (a) CO_2 cloud of constant 1 % concentration, (b) with temp. contours (given only in 500-550 *K* range), and (c) Values of CO_2 concentration and axial velocity, under the ceiling (at $y = H = 0.96$) *(for color image see journal website)*

Conclusions

- The computed field of flow and temperature in the critical ventilation velocity cases, with the critical velocity determined from the experimental study [10], shows a rather good agreement with the expected flow behavior at the critical ventilation regime.
- The effect of the local tunnel velocity field on fire scenario is small in the scaled pasenger vehicle fire size and considerable in a scaled bus (or HGV) fire size.
- For the scaled bus or HGV-vehicle heat release-rate, the effect of a different velocity field approaching the affected tunnel is considerable, with values of CO_2 concentration at scaled person height, averaged horizontally in the tunnel model's portion downstream of the fire source, higher up to 26%, and the temperature increase, measured from the referent value of air-entry temperature, approx. 15% higher - in the skewed velocity field (S4.2) *vs*. the flat field (S4.1.) case.
- The efficiency of momentum transfer for flow field in laboratory model-tunnel (D_h = 0.40 m) with unidirectional vehicle traffic is approx 10% lower than in empty tunnel airflow, with the same ventilation system is $\eta_i \approx 0.71$ [3].

Acknowledgment

The authors would like to thank Ministry of Science of Montenegro, to Faculty of Mechanical Engineering, University of Montenegro, and to Laboratory for Hydraulic Machinery and Energy Systems, Faculty of Mechanical Engineering, University of Belgrade and Project TR35046, for supporting this research.

Nomenclature

A_t – total velocity, [ms^{-1}]
D_f – hub diameter, [m]
D_h – inner pipe diameter, [m]
f – mixture fraction, [–]
k – turb. kinetic energy, [m^2s^{-2}]
Q – heat release rate, [kW]
Re – Reynolds number (= $\rho vc/\mu$), [–]
S – skewness factor, [–]
T – ventilation thrust force [N]
V_t – mean tunnel velocity, [ms^{-1}]
v_r – fan radial velocity, [ms^{-1}]
v_t – fan circum. velocity, [ms^{-1}]
v_z – fan axial velocity, [ms^{-1}]
w – fan mean axial velocity, [ms^{-1}]

Greek symbols

ν – kinematic viscosity, [m^2s^{-1}]
μ – dynamic viscosity [Pa·s]
α – yaw angle [°]
β – pitch angle [°]
η – efficiency of momentum transfer [–]

References

[1] Tarada, F., Design, Testing and Application of an Energy-Efficient Longitudinal Ventilation System, *Proceedings*, 14th International Symposium on Aerodynamics and Ventilation of Tunnels, Dundee, Scotland, UK, Vol. 3, 2011, pp. 103-116
[2] Tarada, F., Brandt, R., Impulse Ventilation for Tunnels – a State of the Art Review, *Proceedings*, 13th International Symposium on Aerodynamics and Ventilation of Vehicle Tunnels, New Brunswick, N. J., USA, May, Vol. 3, 2009, pp. 1067-1070
[3] Šekularac, M. B., Analysis of Flow Fields in Complex Ventilation Systems of Traffic Tunnels (in Serbian), Ph. D. thesis, Faculty of Mechanical Engineering, University of Montenegro, Podgorica, Montenegro, 2015
[4] Levoni, P., *et al.*, Fluid-Dynamic Characterisation of the Mont Blanc Tunnel by Multi-Point Airflow Measurements, *Tunneling and Underground Space Technology*, *48* (2015), Apr., pp. 110-122

[5] Šekularac, M. B., Experimental Determination of Tunnel Ventilation Ducted Fan Performance, *Thermal Science*, *20* (2016), 1, pp. 209-221
[6] Betta, V., *et al.*, Fluid Dynamic Performance of Traditional and Alternative Jet Fans in Tunnel Longitudinal Ventilation Systems, *Tunneling and Underground Space Technology*, *25* (2010), July, pp. 415-422
[7] Colella, F., *et al.*, Multiscale Modeling of Transient Flows from Fire and Ventilation in Long Tunnels, *Computers and Fluids*, *51* (2011), Dec., pp. 16-29
[8] ***, Fluent solver theory guide, Ansys 2013, https://uiuc-cse.github.io/me498cmfa15/lessons/fluent/refs/ANSYS%20Fluent%20Theory%20Guide.pdf
[9] Barbato, L., *et al.*, Fire Safety Investigation for Road Tunnel Ventilation Systems – An Overview, *Tunneling and Underground Space Technology*, *43*, (2014), July, pp. 253-265
[10] Wu, Y., Bakar, M., Control of Smoke Flow in Tunnel Fires Using Longitudinal Ventilation Systems – A Study of the Critical Velocity, *Fire Safety Journal*, *35* (2000), 4, pp. 363-390

Paper submitted: March 14, 2016
Paper revised: April 22, 2016
Paper accepted: April 30, 2016